

Nanostructured flexible Mg-modified LiMnPO₄
matrix as high-rate cathode materials for Li-ion
batteries†Cite this: *J. Mater. Chem. A*, 2014, 2,
6368Received 7th February 2014
Accepted 19th March 2014Qi Lu,^a Gregory S. Hutchings,^a Yang Zhou,^b Huolin L. Xin,^c Haimei Zheng^c
and Feng Jiao^{*a}

DOI: 10.1039/c4ta00654b

www.rsc.org/MaterialsA

One-dimensional (1D) electrode materials have attracted much attention recently because of their potential application in flexible battery technology. Many 1D anode materials based on carbon and metal oxides have been synthesized for flexible batteries, however only limited studies on the cathode side have been conducted. Here, we report the synthesis of high-rate cathode electrodes based on Mg-modified LiMnPO₄ nanofibers. The nanofibers are embedded inside a nanostructured conducting carbon matrix to enhance their electronic conductivity and structural integrity while retaining flexibility. As a result, a 50% increase in capacity is obtained, achieving an outstanding performance of 135 mA h g⁻¹ at a C/10 rate (15 mA g⁻¹). This nanostructured Mg-modified LiMnPO₄ matrix also exhibited superior rate capability and much better cycleability compared to its LiMnPO₄ counterpart. Even at a high charge/discharge rate of 5C (750 mA g⁻¹), 80% of the capacity (107 mA h g⁻¹) is still retained, representing, to the best of our knowledge, the best rate performance for LiMnPO₄-based electrodes. More importantly, such a superior rate capability is achieved with an excellent cycleability (no capacity fading for 200 deep cycles).

Electronic systems that can cover large areas on flexible substrates have received increasing attention in the past few years, because they enable classes of applications that lie outside those easily-addressed with wafer-based electronics.^{1–3} As the critical component for flexible electronics, a flexible energy storage device is crucial because all the functionalities onboard rely on the power supply. The performance of the current generation is greatly limited by the electrode materials,

and many efforts have been devoted to development of high performance flexible batteries.^{4–9} Recently, compliant materials on curvilinear surfaces, such as carbon nanotubes,¹⁰ carbon nanofibers,¹¹ graphene,¹² metal oxide-based nanowires,¹³ and slurry-type mixtures of nanostructured active materials,¹⁴ have been explored as flexible battery electrodes. However, these studies have mainly focused on anode electrode materials, and there has been very limited progress on cathode materials for flexible batteries. It is critical to explore cathode electrode materials with the potential to couple with the developed flexible anodes for device applications. Electrode materials with one-dimensional (1D) nanostructures are the most important candidates in this scenario because of the mechanical flexibility they usually provide.

LiMPO₄ (M = Fe and Mn) materials are of great interest as promising cathode materials in lithium-ion batteries due to their low cost and good stability.^{15–23} However, the rate capability of LiMPO₄ is greatly limited by its intrinsically low electrical and ionic conductivities.^{24–28} For LiFePO₄, the obstacles were overcome by reducing the size of LiFePO₄ particles to nanoscale and introducing a conductive surface coating such as amorphous carbon. These efforts led to the commercialization of LiFePO₄ as a cathode material.^{29–31} Compared with LiFePO₄, LiMnPO₄ possesses a higher lithium ion intercalation potential of 4.1 V *versus* Li/Li⁺ (3.5 V for LiFePO₄), providing about 20% higher energy density than that of LiFePO₄.^{32,33} More importantly, the 4.1 V working potential is compatible with most of the liquid electrolytes that are currently in use, while the working potentials for LiCoPO₄ and LiNiPO₄ (4.8 V and 5.1 V, respectively) are too high for safe operation. Nevertheless, the electronic conductivity of LiMnPO₄ is many orders smaller in magnitude than that of LiFePO₄, which is already insulating, making it challenging to achieve high rate performance for LiMnPO₄ using methods developed for LiFePO₄.³⁴ As an additional challenge, the large volumetric change between LiMnPO₄ and delithiated MnPO₄ during charge/discharge inhibits a smooth lithium ion transport, which results in both lower capacity and limited rate capability.^{32,35}

^aDepartment of Chemical and Biomolecular Engineering, University of Delaware, Newark, DE 19716, USA. E-mail: jiao@udel.edu^bDepartment of Physics and Astronomy, University of Delaware, Newark, DE 19716, USA^cMaterial Science Division, Lawrence Berkeley National Laboratory (LBNL), Berkeley, CA 94720, USA† Electronic supplementary information (ESI) available: SEM of LiMnPO₄ precursor, TEM and HRTEM of LiMnPO₄, STEM-EELS mappings, SEM and TGA data of LiMg_{0.05}Mn_{0.95}PO₄ and LiMnPO₄. See DOI: 10.1039/c4ta00654b

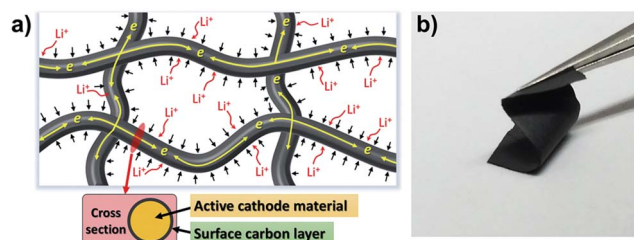


Fig. 1 (a) A schematic diagram and (b) an optical image of the flexible carbon matrix infiltrated with Mg-modified LiMnPO_4 .

In the current work, we report a successful preparation of a nanostructured conducting carbon matrix infiltrated with Mg-modified LiMnPO_4 as composite cathode electrodes for lithium-ion battery applications. The homogeneous conducting carbon matrix achieved provides efficient electron transport channels, while the nanoscaled size, extended and continuous network facilitates ionic transportation and eliminates the occurrence of intergranular voids. A schematic diagram to represent the design concept is presented in Fig. 1. By introducing a small amount of Mg substitution, the volume change across the two-phase interface is effectively reduced. A high capacity of 135 mA h g^{-1} (at C/10 rate), a high capacity retention (80% at 5C), and excellent cycle performance are achieved simultaneously.

An electrospinning technique followed by a calcination process in inert atmosphere was developed for material synthesis. The morphology of the obtained $\text{LiMg}_{0.05}\text{Mn}_{0.95}\text{PO}_4$ and LiMnPO_4 materials are visible in the microscopic images shown in Fig. 2 and S1†. The as-prepared materials were composed of as-spun fibers (Fig. 2a and S1a†) that were long and continuous, with a uniform diameter of approximately 100 nm. The post-calcination process produced the desired C/ $\text{LiMg}_{0.05}\text{Mn}_{0.95}\text{PO}_4$ and C/ LiMnPO_4 composite material network (Fig. 2b and S1b†), accompanied by a slight shrinkage of diameter of the network ligament (Fig. 2c and S1c†). The inert atmosphere during calcination ensured the formation of a homogeneous carbon matrix, infiltrated by the phosphate materials with intrinsically low electrical conductivity. The carbon layer coating was uniform with approximate thickness of 2–4 nm of which the characteristic images are shown in Fig. 2d and S1d.† This is believed to be able to enhance the conductivity of the composite while being thin enough to not interfere with the transport of lithium ions.^{30,31}

Electron energy loss spectroscopy (EELS) characterizations were performed on both $\text{LiMg}_{0.05}\text{Mn}_{0.95}\text{PO}_4$ and LiMnPO_4 materials (Fig. 3). As shown in Fig. 3b, no significant changes in the near edge fine structures of Mn were observed for $\text{LiMg}_{0.05}\text{Mn}_{0.95}\text{PO}_4$ and LiMnPO_4 compared with MnO , except for instrumental broadening. This indicates that $\text{LiMg}_{0.05}\text{Mn}_{0.95}\text{PO}_4$ shares a same Mn bonding environment as that in LiMnPO_4 , and is not significantly deviated from that of Mn^{2+} octahedra in MnO .³⁴ Energy dispersive spectroscopy (EDS) analysis on $\text{LiMg}_{0.05}\text{Mn}_{0.95}\text{PO}_4$ further indicates a successful doping of Mg is achieved because Mg is uniformly distributed throughout the same region as the other elements, P and Mn (Fig. 4).

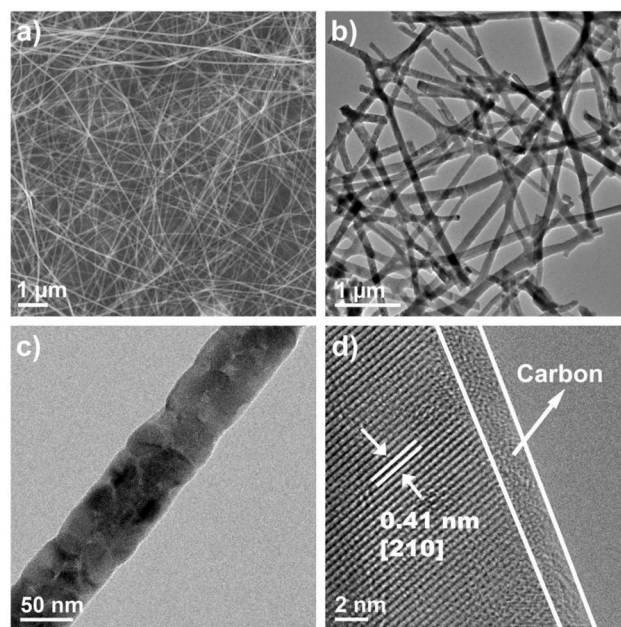


Fig. 2 (a) Scanning electron micrograph (SEM) of as-spun fiber containing precursors for $\text{LiMg}_{0.05}\text{Mn}_{0.95}\text{PO}_4$. (b) Transmission electron micrograph (TEM) of nanostructured $\text{LiMg}_{0.05}\text{Mn}_{0.95}\text{PO}_4$ network. (c) TEM of an individual $\text{LiMg}_{0.05}\text{Mn}_{0.95}\text{PO}_4$ ligament. (d) High resolution TEM (HRTEM) of the surface of an individual $\text{LiMg}_{0.05}\text{Mn}_{0.95}\text{PO}_4$ ligament.

The crystalline structures of both $\text{LiMg}_{0.05}\text{Mn}_{0.95}\text{PO}_4$ and LiMnPO_4 materials were studied with powder X-ray diffraction (PXRD, Fig. 5). The Mg-doped sample showed a very similar profile to that of the undoped sample except for a peak shift towards higher diffraction angles, indicating the desired smaller unit cell volume. The (311) peaks shown with higher magnification in the inset of Fig. 5 clearly illustrate this feature. Every peak in both profiles could be indexed into an orthorhombic structure, space group $Pnma$. No impurity was observed. Refinement of the two PXRD patterns was conducted using the Rietveld approach implemented in the software package PDXL (Rigaku). The experimental and the calculated data agree with each other well. The lattice parameters obtained from the refined pattern are shown in Table 1. It clearly shows that the substitution of a small portion of Mg ions results in a successful reduction of the unit cell volume from 304.02 \AA^3 for LiMnPO_4 to 302.52 \AA^3 for $\text{LiMg}_{0.05}\text{Mn}_{0.95}\text{PO}_4$, which is due to the smaller size of Mg^{2+} (0.86 \AA) compared to Mn^{2+} (0.98 \AA). Additionally, the Mg^{2+} size is larger than that of Mn^{3+} (0.785 \AA) in the delithiated phase, and therefore a reduction of volume contraction during lithiation/delithiation is believed to be achieved.^{37,38}

The electrochemical performance of both electrode materials was evaluated between 2.5 and 4.5 V vs. Li/Li^+ at various C rates ($1\text{C} = 150 \text{ mA h g}^{-1}$). During the charge cycles, cells were trickle charged at the upper voltage limit until the current rate reached C/20. Fig. 6a shows the typical voltage profiles for both LiMnPO_4 and $\text{LiMg}_{0.05}\text{Mn}_{0.95}\text{PO}_4$. While their profiles were similar in shape, the capacity performance was significantly



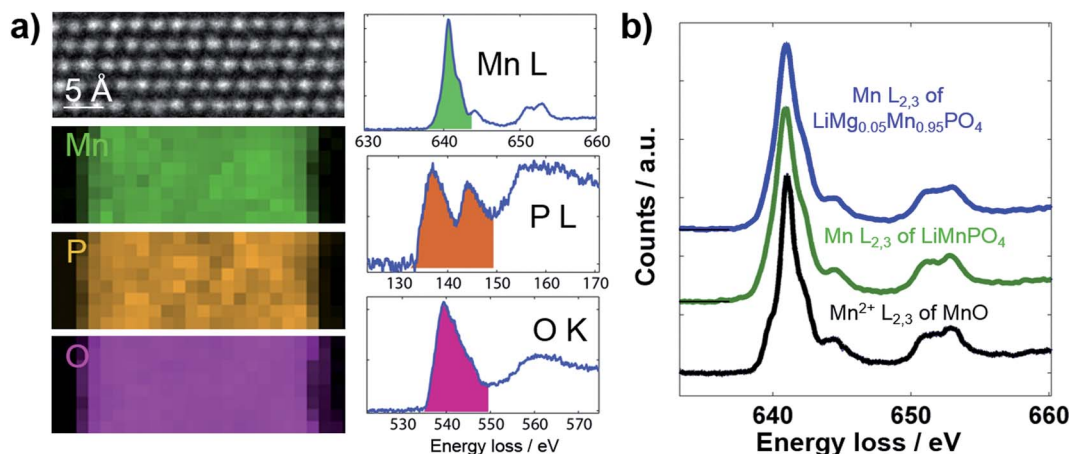


Fig. 3 (a) Scanning transmission electron microscopic EELS (STEM-EELS) mapping of Mn, P, and O in LiMnPO₄. (b) Comparison of Mn L_{2,3} ($2p \rightarrow 3d$) near-edge fine structures of in LiMg_{0.05}Mn_{0.95}PO₄, LiMnPO₄ and MnO. The reference spectrum of MnO was obtained from ref. 6.

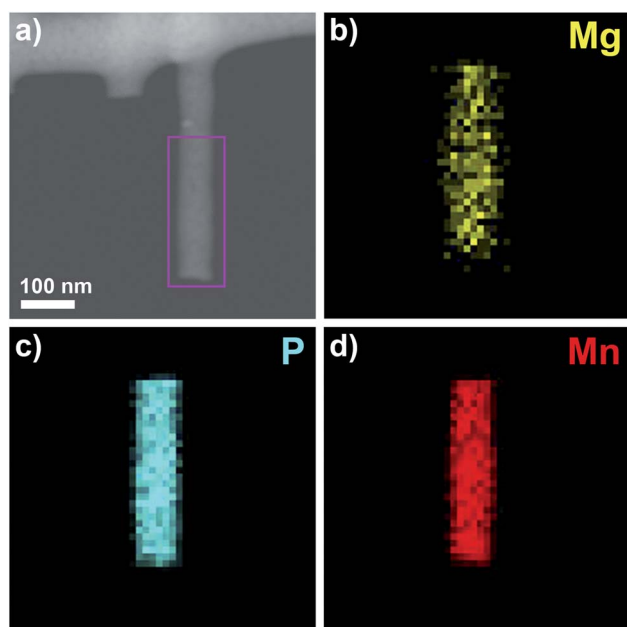


Fig. 4 The EDS mappings of Mg, P and Mn elements on an individual LiMg_{0.05}Mn_{0.95}PO₄ ligament.

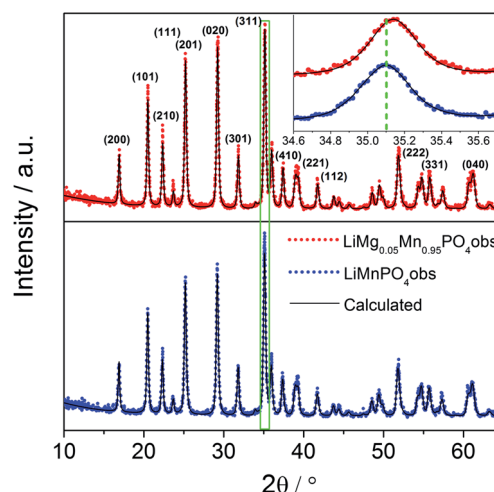


Fig. 5 PXRD patterns and associated Rietveld refinement of LiMg_{0.05}Mn_{0.95}PO₄ and LiMnPO₄ materials. Inset: peaks corresponding to (311) with higher magnification.

Table 1 The difference of lattice parameters for LiMg_{0.05}Mn_{0.95}PO₄ and LiMnPO₄ materials

Material	<i>a</i> /Å	<i>b</i> /Å	<i>c</i> /Å	<i>V</i> Å ³
LiMg _{0.05} Mn _{0.95} PO ₄	10.446(3)	6.1027(19)	4.7457(18)	302.52(18)
LiMnPO ₄	10.4645(17)	6.1141(10)	4.7516(9)	304.02(9)

different. At a discharge rate of C/10, LiMnPO₄ achieved a capacity of less than 90 mA h g⁻¹. However, with only 5% substitution of Mg, LiMg_{0.05}Mn_{0.95}PO₄ achieved a dramatically improved capacity of approximately 135 mA h g⁻¹, which amounts to a greater than 50% enhancement.

As proposed, the increase of capacity of LiMg_{0.05}Mn_{0.95}PO₄ can be attributed to the enhanced electrochemical kinetics due to the reduced volume and reduced structural mismatch across the lithium ion extraction/insertion interface. While the slightly higher discharge potential of LiMg_{0.05}Mn_{0.95}PO₄ (Fig. 6a) might have suggested an improved polarization, electrochemical impedance spectroscopy (EIS) is a more appropriate technique to explore the dynamics at the interface. As shown in Fig. 6b, EIS plots of the LiMg_{0.05}Mn_{0.95}PO₄ and LiMnPO₄ cells at open circuit

potentials were recorded after 10 cycles at C/10 rate. It is clear that the semicircle of LiMg_{0.05}Mn_{0.95}PO₄ cells is significantly smaller than that of LiMnPO₄, indicating a much smaller charge transfer resistance which is responsible for the great improvement of the electrochemical kinetics of lithium ion extraction/insertion.

The voltage profiles of LiMg_{0.05}Mn_{0.95}PO₄ at various charge/discharge rates between C/10 and 6C are presented in Fig. 6c. The un-doped sample showed very similar profiles except for shorter discharge plateaus. Their accordingly calculated cycle capacities are given in Fig. 7. It is clear that LiMg_{0.05}Mn_{0.95}PO₄



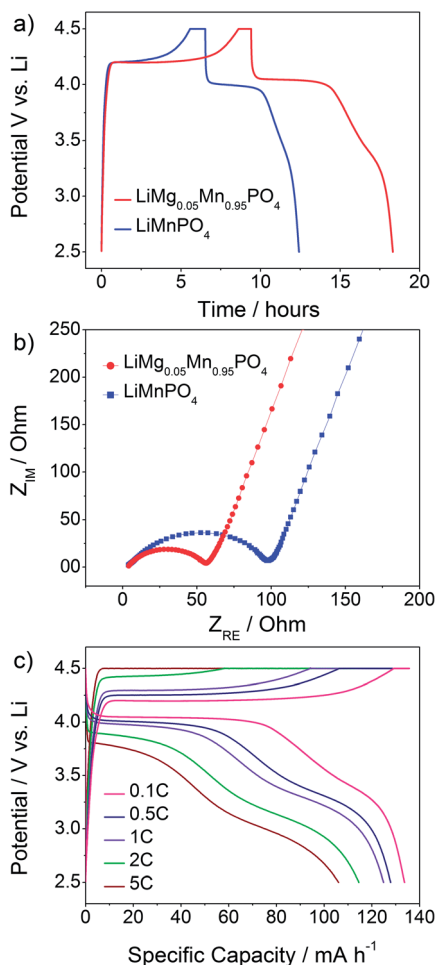


Fig. 6 (a) Typical voltage profiles of the LiMg_{0.05}Mn_{0.95}PO₄ cells and LiMnPO₄ cells at a charge/discharge rate of C/10. (b) EIS plots at open circuit voltage of LiMg_{0.05}Mn_{0.95}PO₄ cells and LiMnPO₄ cells after 10 cycles at a charge/discharge rate of C/10. (c) Typical voltage profiles of the LiMg_{0.05}Mn_{0.95}PO₄ cells at various charge/discharge rates (C/10, C/2, 1C, 2C and 5C).

cells possessed much higher reversible capacity than that of LiMnPO₄ cells at all discharge rates. For LiMg_{0.05}Mn_{0.95}PO₄, the initial discharge capacity at C/10 is approximately 141.1 mA h g⁻¹ and it averages about 135 mA g g⁻¹ in the first 10 cycles. For the pure LiMnPO₄, the initial value is only 92.1 mA h g⁻¹ and averages about 88 mA h g⁻¹ in the first 10 cycles. Even at a high discharge rate of 5C, a discharge capacity of 107 mA h g⁻¹ is still retained for LiMg_{0.05}Mn_{0.95}PO₄; for the pure LiMnPO₄, the value is only 71 mA h g⁻¹. The results show a successful achievement of more than 50% capacity increase throughout all charge/discharge rates with only 5% Mg substitution. Benefited by the nanostructured conducting carbon matrix, excellent rate performance and ultra-stable cycle performance were simultaneously achieved with both electrode materials. For a 50 times increase of charge/discharge rate from C/10 to 5C, the capacity retention remains as high as 80%. No capacity fade was observed in a 200 cycle test as shown in Fig. 7. The overall performance represents, to the best of our knowledge, the state-of-the-art for LiMnPO₄-based electrodes.

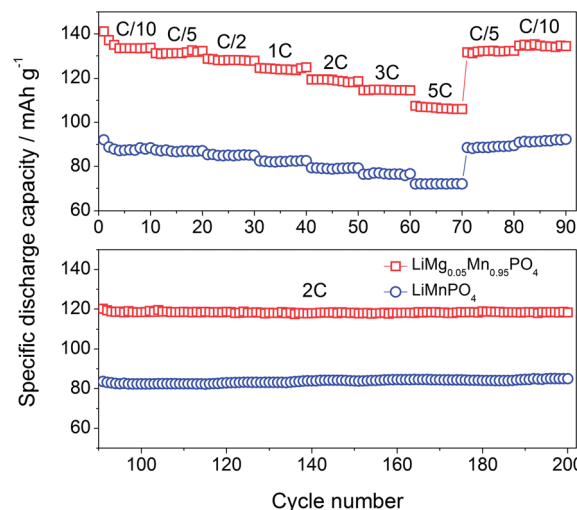


Fig. 7 The cycle performance of the LiMg_{0.05}Mn_{0.95}PO₄ and LiMnPO₄ cells at various discharge rates (from C/10 to 5C).

In summary, the current work presents a successful preparation of nanostructured conducting carbon matrix infiltrated by Mg-modified LiMnPO₄ and its electrochemical application as a lithium-ion battery cathode. The results demonstrate that introducing a small amount of Mg substitution was able to reduce the volume and structural mismatch between the interfaces of lithium ion extraction/insertion without changing the bonding environment of Mn. The improved electrochemical kinetics was responsible for the great enhancement of material charge capacity. The nanostructured conducting matrix ensured a high material utilization, excellent structural integrity, and fast electron/ion transport rate for achieving excellent rate and cycle performance. The developed synthetic strategy provides a potential pathway for fabricating high-performance electrodes for future flexible lithium-ion storage applications.

Experimental section

Synthesis of carbon matrix encapsulated LiMg_{0.05}Mn_{0.95}PO₄ and LiMnPO₄ nanofiber network

To prepare the sol for electrospinning, 0.7795 g LiH₂PO₄ (Sigma-Aldrich, 99%), 1.8826 g Mn(NO₃)₂·4H₂O (Sigma-Aldrich, ≥97.0%), and Mg(NO₃)₂·6H₂O (Sigma-Aldrich, 99%) for achieving desired Mg–Mn ratio were thoroughly mixed in 60 mL de-ionized water using a magnetic stirrer. Poly(ethylene oxide) (1.3 g, Sigma-Aldrich, *M_v* = 600 000) was slowly added to the solution with a stirring speed of 700 rpm. After a homogeneous phase was achieved, 60 μL HNO₃ (Sigma-Aldrich, 70%) was added to the sol to prevent precipitation. The resulting precursor was transferred into a syringe connected to a stainless steel pipetting needle (Cadence Science, 22 × 1-1/2"). A potential of 14 kV (Gamma High Voltage Research) was applied on the needle relative to a grounded rotating drum collector positioned about 10 cm from the tip of the needle. The flow rate of the precursor sol was controlled using a syringe pump (Cole-Parmer) at 0.35 mL h⁻¹. The collected as-prepared fibers were

sandwiched between two silicon wafer substrate, stabilized in a tube furnace at 200 °C for 1 h under H₂ (5 vol%)/Ar (95 vol%) atmosphere, and further calcined at 600 °C for 2 h to obtain the carbon matrix infiltrated with LiMg_{0.05}Mn_{0.95}PO₄ or LiMnPO₄ materials (heating rate 2 °C min⁻¹, cooling rate 5 °C min⁻¹).

Structural characterizations

Powder X-ray diffraction patterns were collected using a Rigaku Ultima IV X-ray diffractometer with Cu K α radiation. SEM studies were performed with a JEOL JSM-6330F. TEM studies and HRTEM studies were performed with a JEOL JEM-2010F using an accelerating voltage of 200 kV. EELS studies were performed with 200 kV field-emission scanning/transmission electron microscope (S/TEM) (Tecnai F20-UT) equipped with Gatan Tridiem electron energy loss spectrometer.

Electrochemical characterizations

The electrochemical performances were evaluated using two-electrode button-type half-cells (CR2032, MTI). The cathode electrodes were prepared by mixing the functional materials with carbon black (Super P, Alfa Aesar) and polyvinylidene fluoride (PVDF) binder (Sigma-Aldrich) with a weight ratio of 75 : 20 : 5 in *N*-methyl-2-pyrrolidone (NMP) solvent (Sigma-Aldrich); the mixture was coated on an Al foil with a doctor-blade technique, dried in a vacuum oven at 60 °C for 24 h, and punched into circular discs 1.5 cm in diameter. Lithium metal (Sigma-Aldrich) was used as the anode electrode. 1.0 M LiPF₆ in ethylene carbonate/dimethyl carbonate/diethyl carbonate (EC/DMC/DEC) (1 : 1 : 1 by volume, MTI Corporation) was used as electrolyte, and polypropylene membranes were used as separators. The complete cells were assembled in a glove box filled with ultrahigh-purity argon. The electrochemical performance of the carbon encapsulated LiMg_{0.05}Mn_{0.95}PO₄ and LiMnPO₄ nanofibers was evaluated with a MACCOR testing system (MACCOR Series 4000) at room temperature. The electrochemical capacity of the samples was calculated based on the total weight of active material and the typical loading density is approximately 5 mg cm⁻². The carbon content of the samples was estimated to be about 2 wt% using a thermogravimetric analyzer (TGA). EIS was carried out using a potentiostat/galvanostat (EG&G Parstat 2273) at open circuit conditions in a frequency range from 0.1 Hz to 100 kHz with an AC signal of 5 mV. All electrochemical measurements were conducted in more than three parallel cells to ensure data reproducibility.

Acknowledgements

The authors are grateful to the University of Delaware Research Foundation (UDRF) for financial support. H. L. Xin and H. M. Zheng acknowledge the support from U.S. Department of Energy (DOE) under Contract # DE-AC02-05CH11231. H. L. Xin thanks Haiyan Tan for supplying the MnO reference spectrum.

References

- 1 D. H. Kim, J. L. Xiao, J. Z. Song, Y. G. Huang and J. A. Rogers, *Adv. Mater.*, 2010, **22**, 2108.
- 2 A. J. Baca, J. H. Ahn, Y. G. Sun, M. A. Meitl, E. Menard, H. S. Kim, W. M. Choi, D. H. Kim, Y. Huang and J. A. Rogers, *Angew. Chem., Int. Ed.*, 2008, **47**, 5524.
- 3 G. Konstantatos and E. H. Sargent, *Nat. Nanotechnol.*, 2010, **5**, 391.
- 4 L. B. Hu, H. S. Kim, J. Y. Lee, P. Peumans and Y. Cui, *ACS Nano*, 2010, **4**, 2955.
- 5 L. B. Hu, H. Wu, F. La Mantia, Y. A. Yang and Y. Cui, *ACS Nano*, 2010, **4**, 5843.
- 6 L. B. Hu, N. Liu, M. Eskilsson, G. Y. Zheng, J. McDonough, L. Wagberg and Y. Cui, *Nano Energy*, 2013, **2**, 138.
- 7 Y. Yang, S. Jeong, L. B. Hu, H. Wu, S. W. Lee and Y. Cui, *Proc. Natl. Acad. Sci. U. S. A.*, 2011, **108**, 13013.
- 8 X. Li and C. Wang, *J. Mater. Chem. A*, 2013, **1**, 165.
- 9 X. Li, A. Dhanabalan, L. Gu and C. Wang, *Adv. Energy Mater.*, 2012, **2**, 238.
- 10 K. Evanoff, J. Benson, M. Schauer, I. Kovalenko, D. Lashmore, W. J. Ready and G. Yushin, *ACS Nano*, 2012, **6**, 9837.
- 11 B. S. Lee, J. H. Seo, S. B. Son, S. C. Kim, I. S. Choi, J. P. Ahn, K. H. Oh, S. H. Lee and W. R. Yu, *ACS Nano*, 2013, **7**, 5801.
- 12 S. M. Paek, E. Yoo and I. Honma, *Nano Lett.*, 2009, **9**, 72.
- 13 B. Liu, J. Zhang, X. F. Wang, G. Chen, D. Chen, C. W. Zhou and G. Z. Shen, *Nano Lett.*, 2012, **12**, 3005.
- 14 D. Y. Wan, C. Y. Yang, T. Q. Lin, Y. F. Tang, M. Zhou, Y. J. Zhong, F. Q. Huang and J. H. Lin, *ACS Nano*, 2012, **6**, 9068.
- 15 G. Y. Chen, J. D. Wilcox and T. J. Richardson, *Electrochem. Solid-State Lett.*, 2008, **11**, A190.
- 16 L. H. Hu, F. Y. Wu, C. T. Lin, A. N. Khlobystov and L. J. Li, *Nat. Commun.*, 2013, **4**, 1687.
- 17 B. Kang and G. Ceder, *Nature*, 2009, **458**, 190.
- 18 J. Kim, H. Kim, I. Park, Y. U. Park, J. K. Yoo, K. Y. Park, S. Lee and K. Kang, *Energy Environ. Sci.*, 2013, **6**, 830.
- 19 K. T. Lee, W. H. Kan and L. F. Nazar, *J. Am. Chem. Soc.*, 2009, **131**, 6044.
- 20 S. M. Oh, S. T. Myung, J. B. Park, B. Scrosati, K. Amine and Y. K. Sun, *Angew. Chem., Int. Ed.*, 2012, **51**, 1853.
- 21 S. W. Oh, S. T. Myung, S. M. Oh, K. H. Oh, K. Amine, B. Scrosati and Y. K. Sun, *Adv. Mater.*, 2010, **22**, 4842.
- 22 Y. G. Wang, Y. R. Wang, E. J. Hosono, K. X. Wang and H. S. Zhou, *Angew. Chem., Int. Ed.*, 2008, **47**, 7461.
- 23 M. S. Whittingham, *Chem. Rev.*, 2004, **104**, 4271.
- 24 P. G. Bruce, B. Scrosati and J. M. Tarascon, *Angew. Chem., Int. Ed.*, 2008, **47**, 2930.
- 25 A. K. Padhi, K. S. Nanjundaswamy and J. B. Goodenough, *J. Electrochem. Soc.*, 1997, **144**, 1188.
- 26 X. H. Rui, X. X. Zhao, Z. Y. Lu, H. T. Tan, D. H. Sim, H. H. Hng, R. Yazami, T. M. Lim and Q. Y. Yan, *ACS Nano*, 2013, **7**, 5637.
- 27 H. K. Song, K. T. Lee, M. G. Kim, L. F. Nazar and J. Cho, *Adv. Funct. Mater.*, 2010, **20**, 3818.
- 28 H. L. Wang, Y. Yang, Y. Y. Liang, L. F. Cui, H. S. Casalongue, Y. G. Li, G. S. Hong, Y. Cui and H. J. Dai, *Angew. Chem., Int. Ed.*, 2011, **50**, 7364.
- 29 W. J. Zhang, *J. Electrochem. Soc.*, 2010, **157**, A1040.



- 30 C. B. Zhu, Y. Yu, L. Gu, K. Weichert and J. Maier, *Angew. Chem., Int. Ed.*, 2011, **50**, 6278.
- 31 R. von Hagen, H. Lorrman, K. C. Moller and S. Mathur, *Adv. Energy Mater.*, 2012, **2**, 553.
- 32 Y. Z. Dong, L. Wang, S. L. Zhang, Y. M. Zhao, J. P. Zhou, H. Xie and J. B. Goodenough, *J. Power Sources*, 2012, **215**, 116.
- 33 D. W. Choi, D. H. Wang, I. T. Bae, J. Xiao, Z. M. Nie, W. Wang, V. V. Viswanathan, Y. J. Lee, J. G. Zhang, G. L. Graff, Z. G. Yang and J. Liu, *Nano Lett.*, 2010, **10**, 2799.
- 34 S. M. Oh, S. W. Oh, C. S. Yoon, B. Scrosati, K. Amine and Y. K. Sun, *Adv. Funct. Mater.*, 2010, **20**, 3260.
- 35 G. Y. Chen and T. J. Richardson, *J. Electrochem. Soc.*, 2009, **156**, A756.
- 36 H. T. Tan, S. Turner, E. Yucelen, J. Verbeeck and G. Van Tendeloo, *Phys. Rev. Lett.*, 2011, **107**, 107602.
- 37 Y. Z. Dong, H. Xie, J. Song, M. W. Xu, Y. M. Zhao and J. B. Goodenough, *J. Electrochem. Soc.*, 2012, **159**, A995.
- 38 G. Y. Chen, A. K. Shukla, X. Y. Song and T. J. Richardson, *J. Mater. Chem.*, 2011, **21**, 10126.

